Author/s:
Ju, Y;Li, S;Tan, AEQ;Pilkington, EH;Brannon, PT;Plebanski, M;Cui, J;Caruso, F;Thurecht, KJ;Tam, C;Kent, SJ

Title:
Patient-Specific Nanoparticle Targeting in Human Leukemia Blood

Date:
2024-10-22

Citation:
Ju, Y., Li, S., Tan, A. E. Q., Pilkington, E. H., Brannon, P. T., Plebanski, M., Cui, J., Caruso, F., Thurecht, K. J., Tam, C. & Kent, S. J. (2024). Patient-Specific Nanoparticle Targeting in Human Leukemia Blood. ACS Nano, 18 (42), pp.29021-29035. https://doi.org/10.1021/acsnano.4c09919.

Persistent Link:
https://hdl.handle.net/11343/353155

ACS NANO

www.acsnano.org

ARTICLE

Patient-Specific Nanoparticle Targeting in Human Leukemia Blood

Yi Ju,* Shiyao Li, Abigail Er Qi Tan, Emily H. Pilkington, Paul T. Brannon, Magdalena Plebanski, Jiwei Cui, Frank Caruso, Kristofer J. Thurecht, Constantine Tam, and Stephen J. Kent*

Cite This: https://doi.org/10.1021/acsnano.4c09919

Read Online

ACCESS | Metrics & More | Article Recommendations | Supporting Information

ABSTRACT: Antibody-directed targeting of chemotherapeutic nanoparticles to primary human cancers holds promise for improving efficacy and reducing off-target toxicity. However, clinical responses to targeted nanomedicines are highly variable. Herein, we prepared and examined a matrix of 9 particles (organic and inorganic particles of three surface chemistries with and without antibody functionalization) and developed an *ex vivo* model to study the person-specific targeting of nanoparticles in whole blood of 15 patients with chronic lymphocytic leukemia (CLL). Generally, anti-CD20-functionalized poly(ethylene glycol) (PEG) nanoparticles efficiently targeted CLL cells, leading to low off-target phagocytosis by granulocytes and monocytes in the blood. However, there was up to 164-fold patient-to-patient variability in the CLL targeting. This was further exemplified through using clinically relevant PEGylated doxorubicin-encapsulated liposomes, which showed high interpersonal differences in CLL targeting (up to 234-fold differences) and off-target phagocytosis (up to 65- and 112-fold differences in granulocytes and monocytes, respectively). Off-target phagocytosis led to almost all monocytes being killed within 24 h of treatment. Variance of the off-target association of PEGylated liposomes with granulocytes and monocytes significantly correlated to anti-PEG immunoglobulin G levels in the blood of CLL patients. A negative correlation between CLL targeting of PEG particles and anti-PEG immunoglobulin M levels was found in the blood. Taken together, our study identifies anti-PEG antibodies as key proteins in modulating patient-specific targeting of PEGylated nanoparticles in human leukemia blood. Other factors, such as the antigen expression of targeted cells and fouling properties of nanoparticles, also play an important role in patient-specific targeting. The human leukemia blood assay we developed provides an *ex vivo* model to evaluate interpersonal variances in response to targeted nanomedicines.

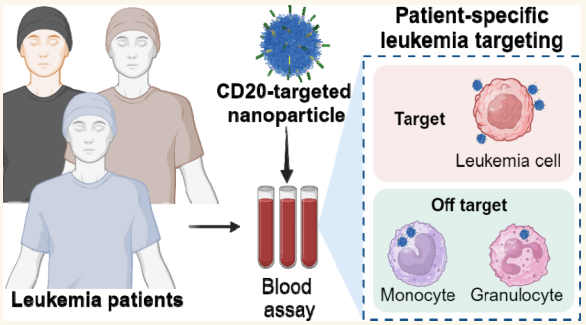

KEYWORDS: *human blood model, off-targeting cytotoxicity, biomolecular coronas, immunoglobulins, precision medicine, particle−immune cell interactions*

Specific tumor targeting by nanoparticles to increase the efficacy of anticancer therapies and reduce off-target effects has been a long-held goal. Recurring issues for nanoparticles are their off-target uptake, clearance, and cytotoxicity to phagocytes such as circulating neutrophils and monocytes.[1] Immune suppression is the major dose-limiting and life-threatening toxicity of chemotherapeutics.[2] A challenge for cancer treatments is providing a more favorable balance between antitumor activity and off-target toxicity.

Efficient targeting of nanoparticles to human cancers is yet to be realized, and improved models of targeting nanoparticles to human cancers are needed to achieve this goal.[3] Recent work has shown the high targeting efficiency of immortalized leukemic cell lines *in vitro* and their efficacy in leukemic cell line-engrafted immunodeficient mice.[4,5] However, *in vitro* studies of tumor cell lines have yet to capture the complexities of targeting primary human cancers in the presence of autologous bystander cells. Furthermore, inbred mouse models typically have restricted immune systems that are developed in pathogen-free environments and rely on the induction or transplantation of tumors on a highly immunodeficient background, which is unlikely to reliably model human malignancy. We previously pioneered a whole human blood model to study the interactions of nanoparticles with immune cells in heathy human blood.[6] The complex mixture of human blood mimics the environment in which particles interact when

Received: July 23, 2024
Revised: September 19, 2024
Accepted: September 23, 2024

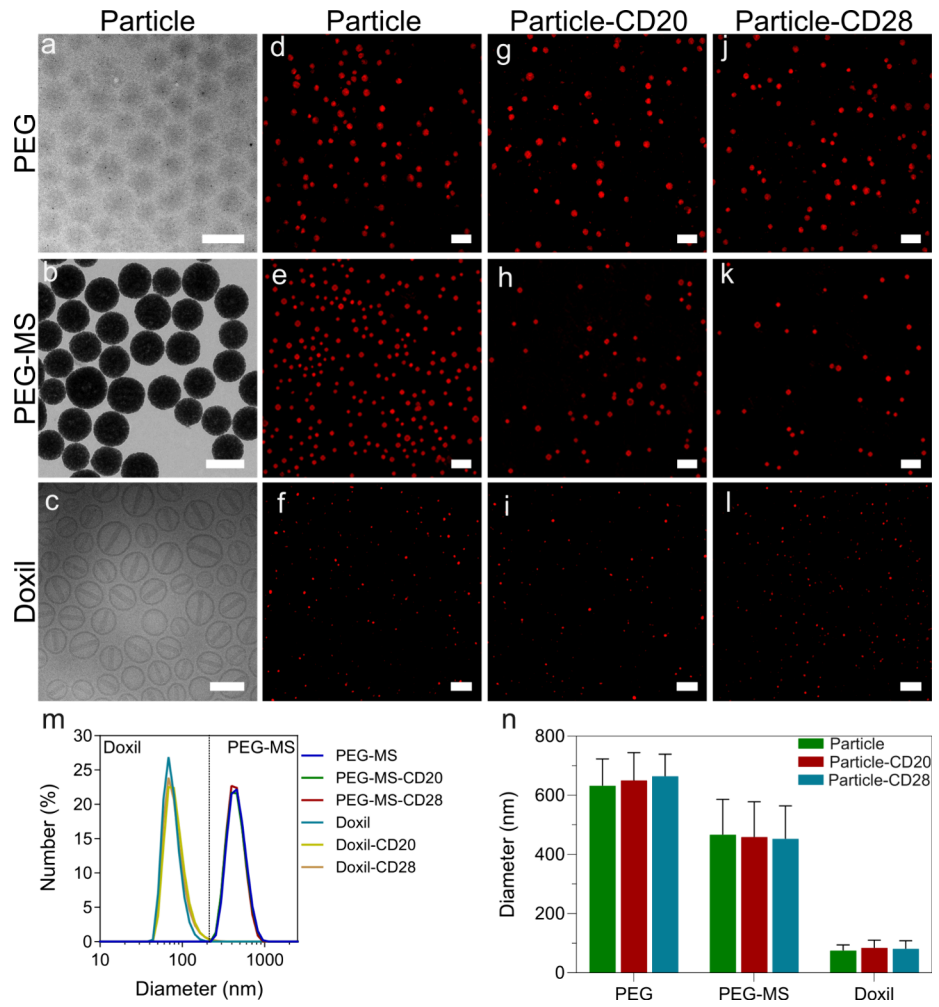

Figure 1. Characterization of PEG, PEG-MS, Doxil nanoparticle systems. (a–c) TEM images of unfunctionalized PEG and PEG-MS nanoparticles and a cryo-TEM image of unfunctionalized Doxil nanoparticles. Scale bars are 500 nm (PEG and PEG-MS) and 100 nm (Doxil). (d–l) SIM images of the three particles types with and without functionalization of anti-PEG/anti-CD20 or anti-PEG/anti-CD28 BsAbs. Scale bars are 2 μm (PEG and PEG-MS nanoparticle systems) and 1 μm (Doxil nanoparticle system). (m) DLS and (n) diameter of PEG-MS and Doxil nanoparticles before and after functionalization with CD20 or CD28 BsAbs. The sizes of the PEG-MS and Doxil (with and without BsAb functionalization) nanoparticles were determined by DLS and presented as the mean ± standard deviation (SD) of three independent measurements. As PEG particles have negligible light scattering, their size was determined by SIM images and shown as the mean ± SD (n = 30). No significant difference in particle size before and after functionalization of BsAbs (two-way analysis of variance with Tukey's multiple comparisons test) was observed.

administered intravenously. However, blood from healthy donors does not usually contain cancer cells, which limits the healthy blood model to assessing only the stealth properties of nanoparticles.

When nanoengineered particles are introduced into the blood, they are immediately subject to recognition and inactivation by the immune system.[7−9] The nanoparticle interactions with blood proteins and immune cells are person-specific, depending on sex, age, genetic background, lifestyle, and underlying health conditions of an individual.[10−12] For example, differences in plasma between cancer patients and healthy subjects has been observed in terms of the composition of the biomolecular corona; these differences were found useful in biomarker discovery and immunomodulation.[13−15] We have previously observed marked variability across healthy human donors in their plasma to modulate protein adsorption and phagocytosis of nanoparticles.[16] However, interpersonal variance among cancer patients on targeting and cytotoxicity of nanoparticles has yet to be investigated. Unraveling the effect of blood variance among cancer patients on bio−nano interactions is expected to lead to rational improvements of nanomedicines and increase their clinical utility.

We reasoned that human blood leukemias provide a milieu in which blood cell tumors cocirculate with other autologous blood cell components, including phagocytes such as neutrophils and monocytes. This provides an *ex vivo*, fully human, outbred model in which the balance of targeting tumors with nanoparticles versus the removal of nanoparticles by phagocytes is assessed. Herein, we recruited patients with chronic lymphocytic leukemia (CLL), a cancer with an abundance of malignant CD20+ B cells in the blood. CLL is a chronic malignancy characterized by a suppressed number of normal B cells but relatively preserved numbers and functions of most other blood immune cells. Fresh blood from patients with CLL was used to study the ability of antibody-functionalized nanoparticles to simultaneously target the B cell tumor and prevent the off-target uptake of particles by

https://doi.org/10.1021/acsnano.4c09919
ACS Nano XXXX, XXX, XXX−XXX

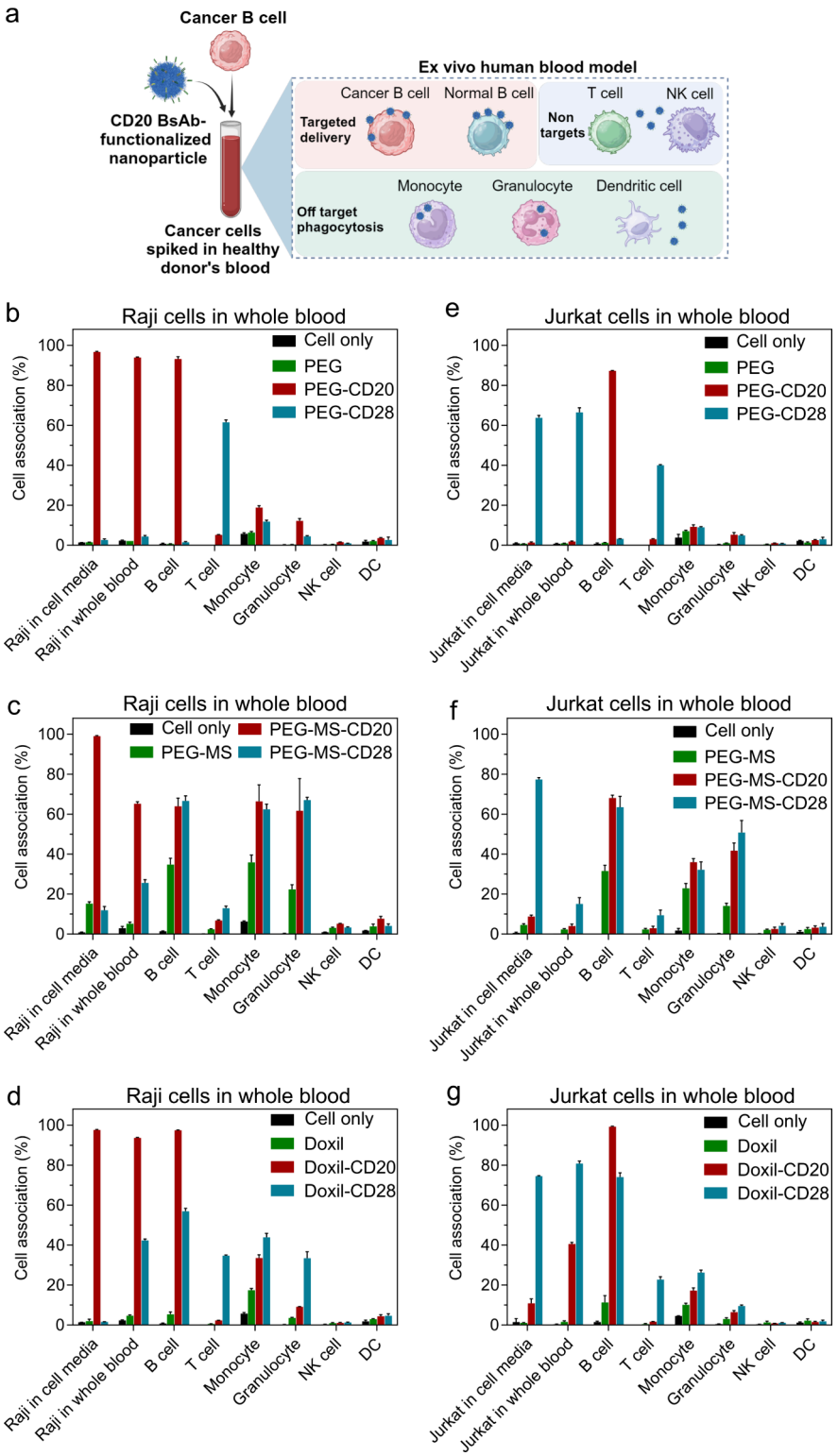

Figure 2. Evaluation of cancer cell targeting in whole human blood model. (a) Schematic illustration of an *ex vivo* human blood model, which was established by spiking cancer cells in healthy human blood to assess nanoparticle cancer targeting in the presence of healthy blood immune cells. Created with BioRender.com. (b–g) Cancer cell targeting of nonfunctionalized and BsAb-functionalized PEG (b, e), PEG-MS (c, f), and Doxil (d, g) nanoparticles in cell culture media versus in whole human blood. Raji (b–d) or Jurkat (e–g) cells were spiked into cell culture media or fresh human blood from a healthy donor, followed by incubation with nanoparticles for 1 h at 37 °C and subsequent analysis by flow cytometry. Cell association (%) refers to the proportion of each cell type with fluorescence above background, stemming from fluorescence-labeled particles (see gating strategy in Figure S3 and S4). Cell association (%) data are shown as the mean ± SD of three independent experiments (using fresh blood from the same donor), with at least 400,000 leukocytes analyzed for each experimental condition studied. Cell only control groups represent the respective cell populations without particle incubation. NK, natural killer cell; DC, dendritic cell.

https://doi.org/10.1021/acsnano.4c09919
ACS Nano XXXX, XXX, XXX−XXX

Table 1. Demographic Information and Cell Count of CLL Patients[a]

Patient ID	Age	Sex	Total WBC ($\times 10^9$ L^{-1})	CLL ($\times 10^9$ L^{-1})	CLL (%) in WBC	CD20+ (%) in CLL	T cell (%) in WBC	CD28+ (%) in T cell
1	90	M	29	19	65	98	6	59
2	56	F	45	31	69	99	8	84
3	66	M	41	32	80	99	1	77
4	49	F	49	35	71	99	9	87
5	67	M	9	1	7	100	27	82
6	79	M	42	33	78	91	2	87
7	74	M	24	14	56	100	9	74
8	78	F	50	36	71	86	1	96
9	64	F	66	48	73	90	4	85
10	51	M	32	23	73	96	3	95
11	58	M	18	11	64	95	11	84
12	73	F	20	11	54	100	12	62
13	68	F	9	3	32	80	11	91
14	55	M	9	6	68	100	14	79
15	73	M	65	50	77	96	2	82
Mean (range)								
	67 (49−90)	60% M	34 (9−66)	24 (1−50)	63% (7−80%)	95% (80−100%)	8% (1−27%)	82% (59−96%)

[a]WBC, white blood cell.

other blood immune cells, particularly granulocytes and monocytes.

RESULTS AND DISCUSSION

Establishing Targeted Nanoparticles and a B and T Cell Tumor Cell Model in Human Blood. To advance the understanding of blood cancer cell targeting, we first established a range of targeted poly(ethylene glycol) (PEG)-based nanoparticles and evaluated their activity when incubated with fresh human donor blood spiked with immortalized B (Raji) or T (Jurkat) cell lines. We previously developed three nanoparticle models spanning a range of high-, medium- or low-fouling materials (Figure 1a−c).[16] Specifically, the nanoparticle models are (1) PEG-functionalized (PEGylated) mesoporous silica (PEG-MS) particles that exhibit high-fouling property; (2) pure PEG particles that show low-fouling property; and (3) PEGylated liposomes containing doxorubicin that show medium-fouling properties between those of the PEG and PEG-MS particles. The PEGylated liposomes containing doxorubicin (referred to simply as Doxil hereafter) were formulated with the same lipid composition and drug/lipid ratio as the liposomal doxorubicin agent Doxil approved by the US Food and Administration (FDA) as a chemotherapy agent. We employed bispecific antibodies (BsAbs) to functionalize the nanoparticles with one antibody arm binding to the PEG on the nanoparticle surface and the other binding to either the B cell marker CD20 or the T cell marker CD28. The use of BsAbs enables a simple functionalization approach for PEGylated particles through noncovalent, antigenic interactions, eliminating the need for complex multistep conjugation chemistries, as demonstrated in our previous study.[17] BsAbs exhibit a strong binding affinity to immobilized PEG with a dissociation constant (K_d) of 20.4 nM for anti-CD20/anti-PEG BsAb,[4] which aligns with the reported affinities for whole IgG1 against PEG.[18] We used T cell targeting as a control for the B cell targeting, in addition to unfunctionalized particles. All three nanoparticle systems efficiently and specifically targeted the relevant B and T cell lines *in vitro* (Figure S1) and CD20 and CD28 expression by B and T cells in human blood was confirmed (Figure S2). The three types of nanoparticles were fully characterized, exhibiting comparable size and polydispersity before and after BsAb functionalization (Figure 1d−n and Table S1). After a 1 h of coculture, flow cytometry (gating strategy is shown in Figure S3 and S4) was used to quantify the targeting of the fluorescently labeled nanoparticles to the B or T cancer cell lines and the association of the nanoparticles with off-target immune cells in the blood, including monocytes and granulocytes (Figure 2a).

When the low-fouling PEG particles functionalized with the anti-CD20 BsAb (PEG-CD20) were incubated with whole blood spiked with Raji B cancer cells, both the Raji B cells and normal B cells were efficiently targeted, and minimal off-target association with phagocytes was observed (Figure 2b). Similarly, when PEG particles functionalized with the anti-CD28 BsAb (PEG-CD28) were incubated with whole blood spiked with the Jurkat T cancer cells, both the Jurkat T cells and normal T cells were efficiently targeted, leading to minimal off-target association with phagocytes (Figure 2e). In contrast, the PEG-MS (Figure 2c,f) and Doxil (Figure 2d,g) particle systems with high- and medium-fouling properties exhibited less efficient targeting and increased off-target uptake by phagocytes. The nanoparticles functionalized with the targeting BsAb generally exhibited greater fouling than the unfunctionalized nanoparticles (Figure 2c,d,f,g), as consistent with previous studies that show that particle surface antibodies can reduce stealthiness.[17,19] These experiments established a range of targeted particles to immortalize B and T cells in the presence of off-target blood cells, thereby enabling the recruitment of human participants for a clinically relevant cancer-targeting model.

Targeting Nanoparticles to Cancerous B Cells in the Blood of CLL Patients. Having established a blood model to assess cancer cell targeting in the presence of healthy blood immune cells, we proceeded to recruit 15 participants with CLL having significant numbers of primary B cancer cells in their blood. In most patients, malignant B cells outnumbered normal white cells in the blood, as expected for CLL patients who are not in remission (Table 1, Figure S5a, b). Almost all malignant B cells (mean 95%, range 80−100%) expressed

https://doi.org/10.1021/acsnano.4c09919
ACS Nano XXXX, XXX, XXX−XXX

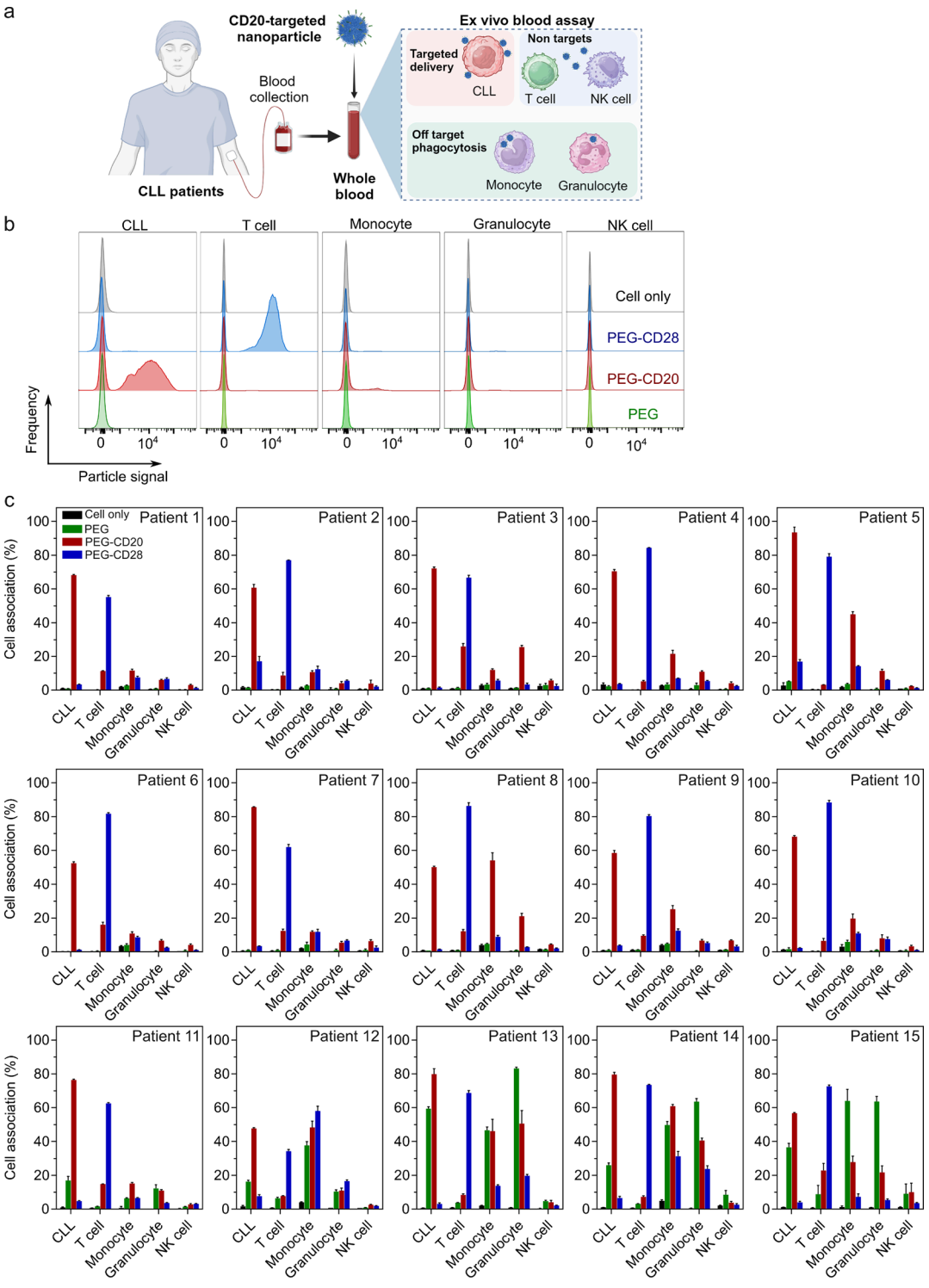

Figure 3. Cancer cell targeting of BsAb-functionalized PEG particles in the whole blood of CLL patients. (a) Schematic illustration of a whole human CLL blood model, where fresh whole blood from CLL patients was collected and subsequently incubated with nanoparticles to assess leukemia targeting in the presence of blood immune cells. Created with BioRender.com. (b) Flow cytometry histograms representing cell association of PEG, CD20-functionalized PEG (PEG-CD20), and CD-28-functionalized PEG (PEG-CD28) particles with targeted CLL and other blood immune cells in the blood from CLL patients. (c) CLL targeting of BsAb-functionalized PEG particles in the whole blood of 15 CLL patients (see Table 1 for patient details). Cell association (%) refers to the proportion of each cell type with fluorescence above background, stemming from fluorescence-labeled particles (see gating strategy in Figure S7). Cell association (%) data are shown as the mean ± SD of three independent experiments (using fresh blood from each donor), with at least 400,000 leukocytes analyzed for each experimental condition studied. Cell only control groups represent the respective cell populations without particle incubation. Patients are identified based on monocyte−PEG particle association (from low to high).

https://doi.org/10.1021/acsnano.4c09919
ACS Nano XXXX, XXX, XXX−XXX

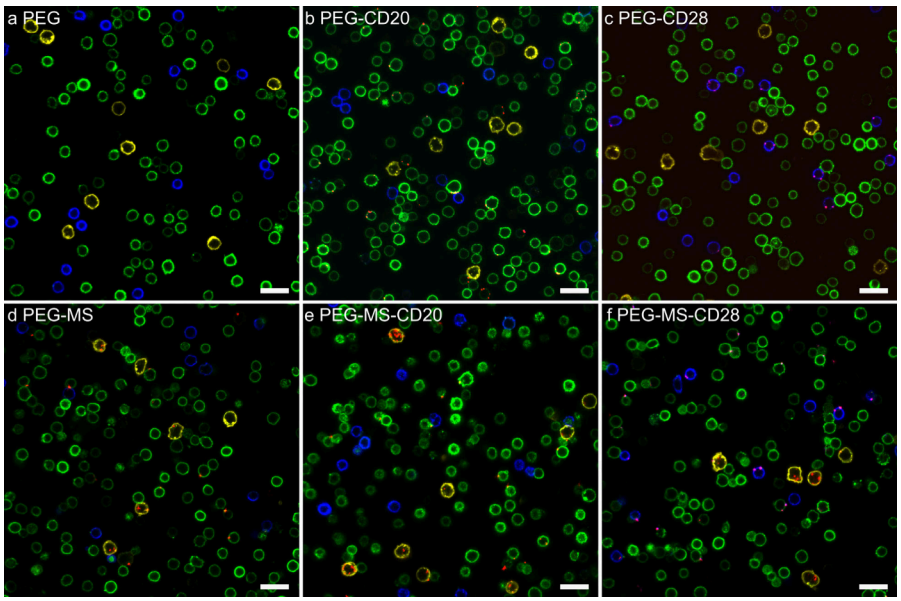

Figure 4. Confocal microscopy images showing the association of BsAb-functionalized PEG or PEG-MS nanoparticles with blood cells from a CLL patient. (a−c) PEG and (d−f) PEG-MS nanoparticles functionalized with or without anti-PEG/anti-CD20 or anti-PEG/anti-CD28 BsAbs were incubated with PBMCs from a CLL patient for 1 h at 37 °C, followed by phenotyping cells with antibody cocktails and imaging by confocal microscopy. Green, CD20+ CLL cells; blue, CD3+ T cells; yellow, CD14+ monocytes; red, fluorescence-labeled PEG or PEG-MS nanoparticles. Scale bars are 20 μm.

CD20 (Figure S5c, Table 1). None or very few normal B cells (<0.5% of the total CD19+ B cell populations) are present in the blood of CLL patients (Figure S6) and thus not included in the targeting study. Normal T cells were present, as expected, with an average of 82% (range 59−96%) of T cells expressing CD28 (Figure S5d), which is the target of control CD28-targeted nanoparticles.

The nine targeted nanoparticles (PEG, PEG-MS, and Doxil with or without functionalization of CD20 or CD28 BsAbs) were incubated with fresh blood from all 15 CLL patients for 1 h at 37 °C (Figure 3a), followed by flow cytometry analysis (Figure 3b; the gating strategy is shown in Figure S7). For most patients, the CD20-functionalized PEG nanoparticles efficiently targeted CLL cells with considerably low off-target association with T cells, monocytes, and granulocytes (Figure 3c). Similarly, the CD28-functionalized PEG nanoparticles targeted T cells with generally minimal off-target association with CLL cells, monocytes, and granulocytes. These results were visually supported by confocal microscopy imaging of blood cells from a CLL patient in Figure 4b. CD20-functionalized PEG nanoparticles (red) were commonly observed on the surface of CLL cells (green) rather than on the surface of T cells (blue) or monocytes (yellow). CD28-functionalized PEG nanoparticles associate primarily with T cells only (Figure 4c), whereas unfunctionalized PEG nanoparticles rarely associate with any of the cells (Figure 4a).

Notably, the PEG nanoparticles with or without BsAb functionalization displayed high association with monocytes and granulocytes in a minority of subjects (patients #11−15 in Figure 3c). Although the targeting of CD20-functionalized PEG nanoparticles was generally maintained, there was substantial interpatient variability in CLL targeting (up to 164-fold difference in cell association mean fluorescence intensity (MFI), Figure S8a) and off-target association with phagocytes (up to 6- and 12-fold difference in cell association% with monocytes and granulocytes, respectively; Figure 5a) across all patients.

In contrast to the PEG particle system, the high-fouling nature of the PEG-MS particle system led to poor targeting and high off-target association across most patients, as observed in Figure S9 and the summary of results across the 15 patients in Figure 5b and Figure S8b. CD20-functionalized PEG-MS nanoparticles (PEG-MS-CD20) displayed minimal specific CLL targeting and high off-target association with monocytes and granulocytes, at similar levels to those observed with PEG-MS and PEG-MS-CD28 nanoparticles. The confocal microscopy images in Figure 4d−f show that many nanoparticles were phagocytosed by monocytes (yellow), whereas a few particles specifically targeted CLL or T cells.

Doxil, which is a clinically used liposomal chemotherapeutic nanoparticle,[20] was examined as the third particle system. The use of Doxil resulted in a large interpersonal difference in targeting to CLL cells in the cohort of patients studied (up to 234-fold difference in the MFI cell association, Figure 5c, Figure S8c). Specific CLL targeting by CD20-functionalized Doxil (Doxil-CD20) was clearly observed in 6 of 15 patients (patients no. 1, 3, 8, 9, 10, 11; Figure S10), while substantial off-target association with monocytes and granulocytes was observed in most patients with a large interpatient variance (up to 65- and 112-fold differences in cell association MFI with granulocytes and monocytes, respectively, Figure S8c). The performance of the three BsAb-functionalized nanoparticle systems (PEG, PEG-MS, and Doxil) was compared to illustrate how particle chemistry had a major effect on targeting and off-target effects (Figure 5d). The large range of targeting and off-target effects across the 15 donors is notable across all three nanoparticle systems and led to experimental work to understand this variability.

PEG Antibodies Are Associated with Higher Off-Target Association with Phagocytes. The large range of off-target association of the PEGylated nanoparticles across the

https://doi.org/10.1021/acsnano.4c09919
ACS Nano XXXX, XXX, XXX−XXX

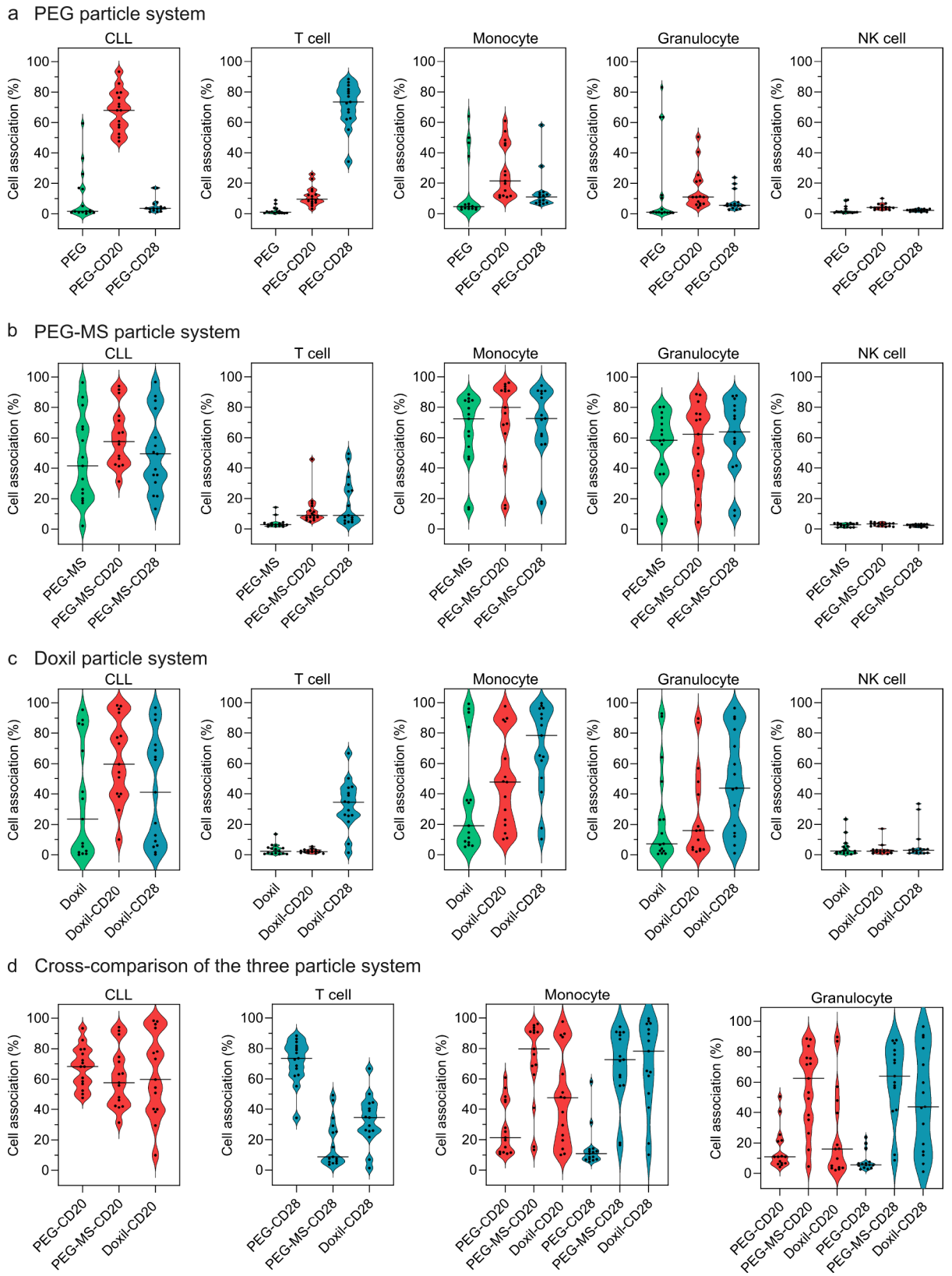

Figure 5. Cell association summary of PEG, PEG-MS, and Doxil nanoparticle systems (with and without BsAb functionalization) in the whole blood of 15 CLL patients. (a–c) Violin plots summarizing the association of nonfunctionalized and BsAb-functionalized PEG, PEG-MS, and Doxil nanoparticles with CLL cells, T cells, monocytes, granulocytes, and NK cells in CLL patient blood after 1 h incubation at 37 °C. (d) Cross-comparison of the three particle systems of their association with CLL cells, T cells, monocytes, and granulocytes in CLL patient blood. Each data point represents the mean of three independent experiments (using the same batch of fresh blood from each donor). The median cell association across 15 CLL patients is shown as a solid line in the violin plots.

https://doi.org/10.1021/acsnano.4c09919
ACS Nano XXXX, XXX, XXX−XXX

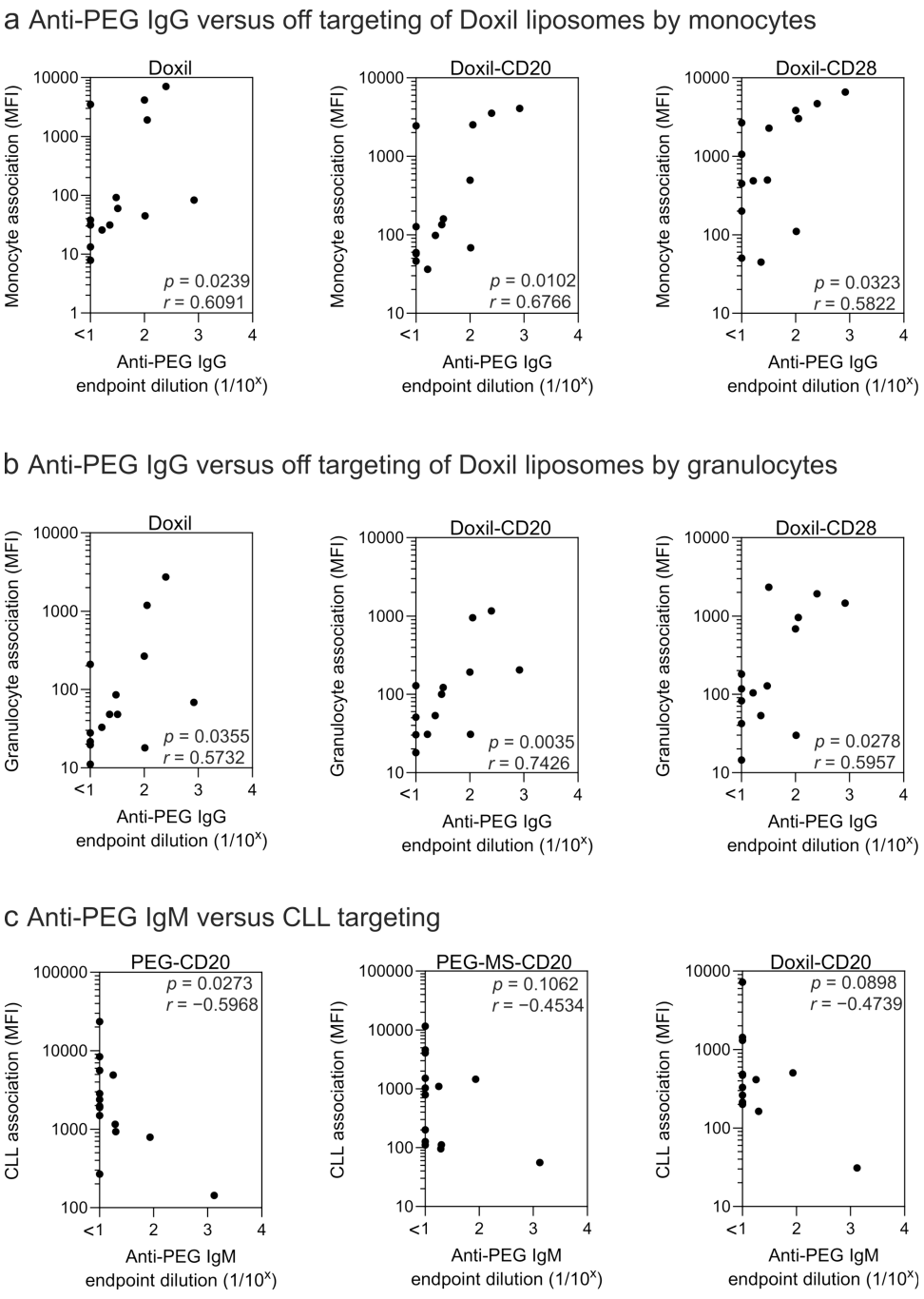

Figure 6. Anti-PEG antibodies influence particle phagocytosis and CLL targeting in the blood of CLL patients. (a,b) Anti-PEG IgG levels in the plasma positively correlate with the phagocytosis of Doxil nanoparticles with and without BsAb (CD20 or CD28) functionalization by monocytes and granulocytes. (c) Anti-PEG IgM levels in the plasma negatively correlate with CLL targeting of CD20-functionalized PEG particles. Cell association (MFI) refers to the median fluorescence index of each cell type, stemming from fluorescence-labeled particles. The anti-PEG IgG and IgM levels in the plasma were determined by ELISA (Figure S11). Statistics were assessed by Spearman correlation analysis (n = 14).

15 CLL patients was consistent with our previous observation on blood samples from 23 healthy donors, where broad interpersonal differences in phagocyte−nanoparticle association were found.[16] That previous study linked interpersonal differences to person-specific biomolecular coronas that formed on the particles, particularly the variance of immunoglobulins present in the coronas. We recently developed methods to quantify PEG-specific antibodies and found that the levels of PEG-specific antibodies induced by SARS-CoV-2 mRNA vaccines in humans correlated with the association of PEGylated lipid nanoparticles with blood phagocytes.[21] This raised the hypothesis that the off-target association of antibody-functionalized nanoparticles could be linked, at least in part, to PEG-specific antibodies binding to and fouling the PEGylated nanoparticles.

We measured the levels of PEG-specific immunoglobulin G (IgG) and immunoglobulin M (IgM) antibodies in 14 CLL patients and found a large interpatient variance (up to 83- and 133-fold differences in the titers of IgG and IgM, respectively; Figure S11). The association of the Doxil nanoparticle system

https://doi.org/10.1021/acsnano.4c09919
ACS Nano XXXX, XXX, XXX−XXX

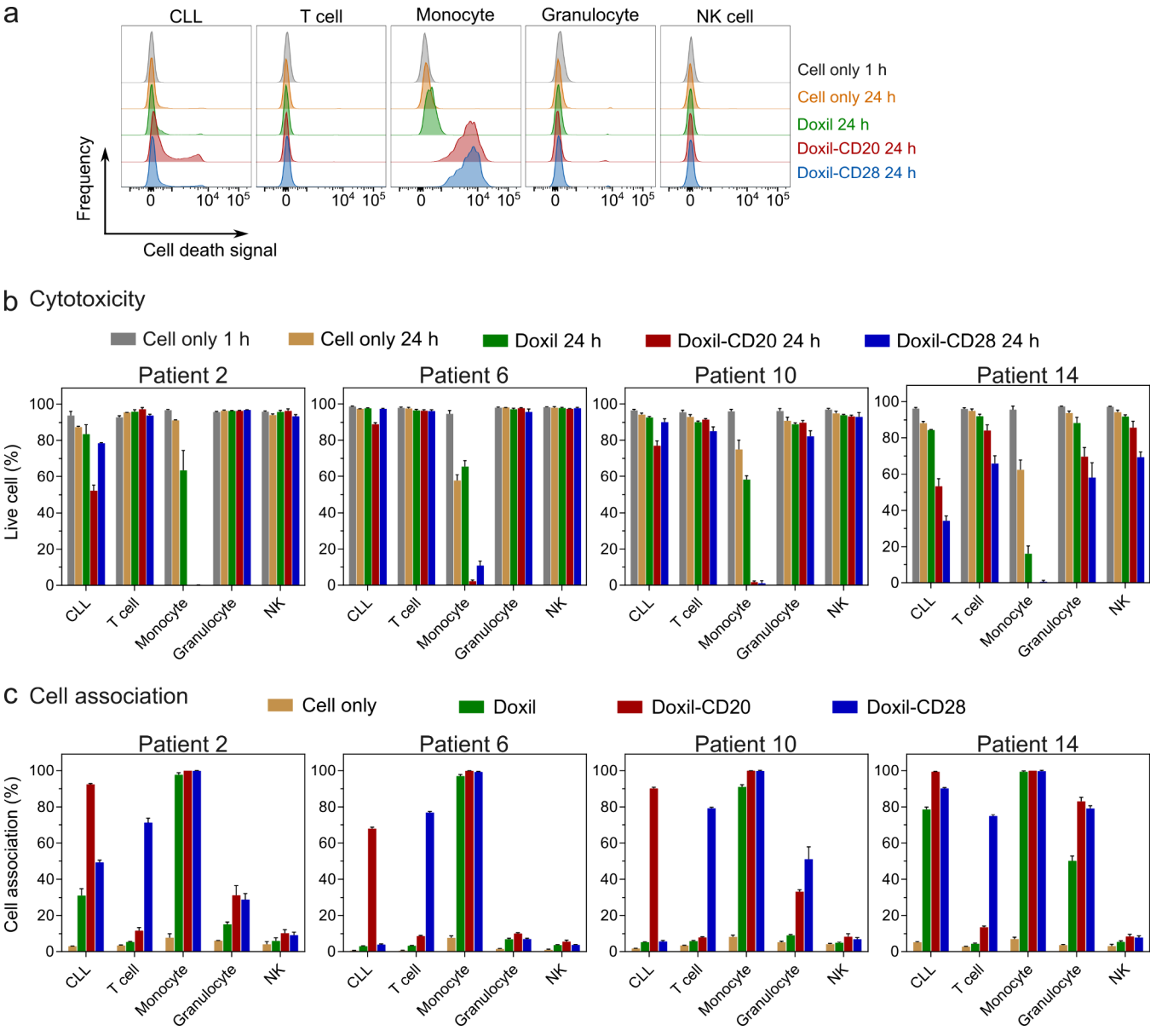

Figure 7. Targeted and off-targeted cytotoxicity of nonfunctionalized and BsAb-functionalized Doxil nanoparticles to CLL and healthy immune cells in blood of CLL patients. (a) Flow cytometry histograms represent the cell death of CLL cells, T cells, monocytes, granulocytes, and NK cells after treating with Doxil nanoparticles in the blood of a CLL patient (Patient 2). (b) Cytotoxicity and (c) cell association of nonfunctionalized and BsAb-functionalized Doxil nanoparticles in the whole blood of four CLL patients. The nonfunctionalized and BsAb-functionalized Doxil nanoparticles were incubated with the whole blood of CLL patients for 24 h at 37 °C, after which the cells were phenotyped with antibody cocktails and dead cells were labeled with SYTOX AADvanced dead cell stain. Data in (b,c) are shown as the mean ± SD of three independent experiments (using fresh blood from each donor), with at least 400,000 leukocytes analyzed for each experimental condition studied.

(with or without functionalization of BsAb) with both granulocytes and monocytes significantly correlated with PEG-specific IgG across the 14 patients (Figure 6a,b), as expected due to the presence of PEG on the surface. No significant correlations between PEG antibodies and the association of PEG or PEG-MS nanoparticles with phagocytes were observed (Figure S12 and S13). The pure PEG particles are low fouling,[22] with 4−8 times less protein adsorption than PEG-MS particles.[23] *In vivo* studies showed that the presence of anti-PEG antibodies did not significantly accelerate the blood clearance of PEG particles, likely due to low opsonin adsorption, including anti-PEG antibodies.[24] In contrast, PEG-MS particles exhibit high fouling with physicochemical properties influenced by their MS cores, as indicated by their negative zeta potential (−31 mV, Table S1). Therefore, the opsonization of PEG-MS particles may be driven not only by anti-PEG antibodies but also by other factors, such as surface charge, pore size, and diameter of the MS.

The influence of PEG-specific antibodies on the CLL targeting of CD20-functionalized particles in whole blood was examined. We hypothesized that higher levels of anti-PEG antibodies could either reduce particle availability through off-target associations with phagocytes or decrease targeting by contributing to the masking of the target antibodies. A significant negative correlation between the level of anti-PEG IgM and CLL targeting of CD20-functionalized PEG particles

https://doi.org/10.1021/acsnano.4c09919
ACS Nano XXXX, XXX, XXX−XXX

was observed, similar to trends observed with CD20-functionalized PEG-MS and Doxil nanoparticles (Figure 6c, Figure S14b). However, reduced targeting was not observed with higher levels of PEG-specific IgG (Figure S14a), suggesting that the binding of larger PEG-specific pentavalent IgM molecules may play a more important role in occluding or sterically hindering the target molecule (BsAb).

Influence of Antigen Expression on Nanoparticle Targeting in Leukemia Blood. In addition to anti-PEG antibodies, we found a large interpatient variance in the levels of CD20 expression on CLL cells (up to 120-fold difference in MFI) and CD28 expression on T cells (up to 5-fold difference in MFI) in blood samples across 15 CLL patients (Figure S5e,f). We hypothesized that higher CD20 expression on CLL cells or CD28 expression on T cells would lead to higher CD20 or CD28 BsAb-mediated nanoparticle targeting, respectively. A significant positive correlation between the level of CD28 expression on T cells and T cell targeting by CD28-functionalized PEG particles was observed (Figure S15a). A similar trend was observed in the correlation between the level of CD20 expression on CLL cells and CLL targeting by CD20-functionalized PEG particles (Figure S15b). However, the targeting of CD20- or CD28-functionalized PEG-MS and Doxil particles did not correlate with CD20 expression on CLL cells or CD28 expression on T cells (Figure S15). Taken together, for low-fouling particle systems such as pure PEG particles, their targeting performance was partly driven by antigen expression on targeted cells. In contrast, higher fouling systems, such as PEG-MS and Doxil particles, are prone to opsonization and are less influenced by target antigen expression.

Cytotoxicity of Targeted Doxil Nanoparticles to Both CLL Cells and Phagocytes. The goal of chemotherapy is to kill the tumor while minimizing the off-target killing of healthy immune cells. We further advanced our whole blood CLL model to study cytotoxicity of the Doxil nanoparticle system *ex vivo* across four patients (randomly selected according to availability). A longer incubation period (24 h) was employed to monitor potential cell death. Both the killing and targeting of CLL and other blood cells were simultaneously examined by employing a dead cell stain and flow cytometry after the incubation of the Doxil nanoparticles (which contain the chemotherapeutic agent doxorubicin) with whole blood (Figure 7a). In patients nos. 2, 6, 10, and 14, we observed nearly complete death of monocytes after treatment with the CD20- or CD28-functionalized Doxil nanoparticles, whereas cell death by unfunctionalized Doxil was reduced to a considerably lower degree (Figure 7b). The death of monocytes was consistent with their high uptake of Doxil nanoparticles and their sensitivity to doxorubicin (Figure 7c). Only modest targeted killing of the CLL cells was observed after 24 h of incubation with CD20-functionalized Doxil nanoparticles (9−31% killing over unfunctionalized Doxil). This likely reflects the limited intracellular uptake of Doxil liposomes by CLL cells, as well as the relative resistance of CLL cells to doxorubicin. Patient #14 displayed no specific targeting—this subject displayed a high uptake of all three nanoparticles by phagocytes and incidentally had high levels of PEG IgG. Overall, the data are consistent with a model in which phagocytes are commonly killed through off-target uptake by high-fouling nanoparticles, potentially facilitated through opsonization by PEG-specific antibodies.

CONCLUSIONS

The safety and effectiveness of chemotherapy are limited largely by off-target effects on the healthy immune system. We developed a fully human *ex vivo* model of targeting a primary human B cell malignancy (CLL) in the presence of immune cells within the blood. This model allowed for the identification of important issues related to targeting human cancers with antibody-functionalized nanoparticles.

We observed a large patient-to-patient variance in the capacity of nanoparticles to target primary human cancer cells in blood and avoid off-target uptake and the killing of phagocytes. Anti-PEG antibodies were identified as key plasma proteins modulating this variance. It has been reported that anti-PEG antibodies bind to the surface of PEGylated nanoparticles, leading to the binding and activation of complement proteins.[25] This cascade likely results in the formation of an anti-PEG antibody-mediated biomolecular corona around PEGylated nanoparticles such as PEG-MS and Doxil nanoparticles used in this study. Indeed, we previously identified immunoglobulins and complement proteins as key components of the biomolecular corona modulating interactions of 100 nm PEG-MS nanoparticles with circulating phagocytes.[16] The *in vivo* formation of biomolecular coronas on Doxil in human blood has been previously described.[26] It has been demonstrated that the composition of biomolecular coronas significantly influences the fate and application of lipid nanoparticles.[27−29] PEG antibodies and the associated biomolecular coronas bound to antibody-functionalized nanoparticles are likely to sterically hinder the ability of a targeting antibody to bind to its ligand, leading to reduced targeting efficiency, a phenomenon that has been observed in other types of PEGylated targeted nanoparticles.[30]

In this study, we found that CLL patients with low levels of anti-PEG antibodies had a greater targeting efficiency of antibody-functionalized PEGylated nanoparticles and lower off-target phagocyte association. Our results suggest that patients with low levels of PEG-specific antibodies will respond more effectively and safely to targeting nanotherapeutics that contain PEG. For subjects with higher levels of PEG antibodies, improved low-fouling PEG-free nanoparticles are needed, a field of considerable interest.[31,32] The widespread use of PEG in cosmetics and other materials,[33,34] as well as the incorporation of PEG in current SARS-CoV-2 mRNA vaccines,[35] may possibly increase population levels of anti-PEG antibodies, resulting in poor responses to anticancer therapies based on PEGylated nanoparticles in the future. Clinical studies on PEGylated protein drugs have reported that PEG-specific antibodies can reduce treatment efficacy and cause adverse reactions.[36−39]

We also observed distinct patterns across the three nanoparticle systems studied that have implications for future cancer nanotherapeutics. Low-fouling nanoparticles, such as the pure PEG particles,[22,40] were critical for achieving high targeting and low off-target association in most patients. On the other hand, the CD20-functionalized PEG-MS and Doxil nanoparticles, even in the absence of high levels of anti-PEG antibodies, generally exhibited low targeting efficiency and high off-target effects in blood due to their relatively high fouling properties. The levels of antigen expression on targeted cells influenced the targeting performance of PEG particles but not PEG-MS or Doxil particles. This highlights that the fouling properties of nanoparticles, antigen expression on cells, and

https://doi.org/10.1021/acsnano.4c09919
ACS Nano XXXX, XXX, XXX−XXX

anti-PEG antibody levels in blood all play important roles in influencing the patient-specific targeting of nanoparticles. In this study, CD20- and CD28-functionalized PEG particles showed potential in targeting CLL and T cells in human leukemia blood, respectively. Future studies using smaller PEG nanoparticles (e.g., those with a diameter of ~100 nm)[6,17] are required to examine their targeting performance *in vivo*.

Monocytes phagocytosed antibody-functionalized Doxil and were killed within 24 h of *ex vivo* incubation, which is consistent with the overall high toxicity of Doxil liposomes observed clinically.[41] In contrast, fewer than half of the number of CLL cells were specifically killed by CD20-functionalized Doxil liposomes within a similar time frame. Although disappointing, these results provide an *ex vivo* benchmark upon which to improve the targeting and reduce the off-target effects of emerging chemotherapeutic nanoparticles. Each *ex vivo* test of both targeting and off-target effects requires only 100 μL of blood, providing a system with a reasonable throughput for the rational selection of improved cancer nanotherapeutics.

Overall, we provide an *ex vivo* human leukemia blood model that allows the simultaneous study of the cancer targeting and cytotoxicity of nanoparticles. The stealth properties of nanoparticles and anti-PEG antibody levels in the plasma were major determinants of successful cancer targeting and reduced off-target cytotoxicity on healthy immune cells. The findings of this study are expected to guide the development of improved cancer targeted nanoparticles and the improved selection of patients for personalized treatments.

METHODS

Ethics. The study protocols were approved by the University of Melbourne and Royal Melbourne Hospital Human Research Ethics Committee (#2057981.1, 13/36, 22993−34586−3) and all associated procedures were carried out in accordance with the approved guidelines. All subjects provided written informed consent.

Preparation and Characterization of BsAb-Functionalized Particles. Alex Fluor 647 (AF647) or AF555-labeled PEG-MS and PEG particles were prepared using a previously published method.[16] Dioctadecyl-3,3,3,3-tetramethylindodicarbocyanine (DiD)-labeled PEGylated doxorubicin-encapsulated liposomes that were formulated with the same lipid composition and drug/lipid ratio as FDA-approved liposomal doxorubicin agent (Doxil), and the addition of DiD (0.2 mol %), were purchased from FormuMax Scientific Inc., USA and referred to Doxil nanoparticles in the present study. BsAbs were synthesized using a previously published method.[4,42] The size of BsAbs and their binding affinity against immobilized PEG has been previously reported.[4] The functionalization of BsAb on particles was performed according to a previously published method with slight modification.[17] Briefly, PEG particles (5×10^9), PEG-MS particles (10^9), or Doxil (100 μg based on lipid concentration) were incubated with BsAb (50 μg) in phosphate-buffered saline (PBS) at 4 °C under orbital mixing for 15 h. Transmission electron microscopy (TEM) images of PEG and PEG-MS particles were acquired by using an FEI Tecnai TF20 microscope at an operation voltage of 120 kV under liquid nitrogen cooling. For analysis, PEG and PEG-MS particle suspensions were dropped and air-dried on Formvar carbon-coated copper grids (plasma-treated). Cryogenic TEM (Cryo-TEM) images of Doxil particles were acquired by using a FEI Tecnai Spirit microscope at an operation voltage of 120 kV under liquid nitrogen cooling under low dose conditions. Doxil suspensions were applied to glow-discharged lacey carbon grids and vitrified by using a Vitrobot (FEI) system. Vitrified sample grids were stored in liquid nitrogen prior to imaging. Super-resolution structured illumination microscopy (SIM) was performed on a Zeiss Elyra 7 Lattice SIM equipped with a 63×/1.4 NA Plan-Apochromat oil immersion objective lens, a pcoedge sCMOS 4.2 CL HS camera, and a 642 nm excitation laser. Image acquisition and SIM reconstruction were performed with Zeiss ZEN Black 3.1 SR software. Dynamic light scattering (DLS) analysis of the particles was performed on a Zetasizer Nano-ZS (Malvern Instruments, UK) instrument. Zeta-potential measurements of the particles were performed at pH 7.4 in phosphate buffer (5 mM) using a Zetasizer Nano-ZS. Particle counting for PEG and PEG-MS particles was performed using an Apogee A50-Micro flow cytometer (Apogee Flow Systems, UK). The concentration of Doxil (based on the lipid concentration) was provided by the manufacturer.

Evaluation of Cancer Cell Targeting Using Cell Lines *In Vitro*. Raji, Jurkat, Hut-78, and THP-1 cell lines were purchased from the American Type Culture Collection (USA) and maintained in complete RPMI-1640 medium containing 10% fetal calf serum (FCS) and GlutaMAX at 37 °C in a cell culture incubator with 5% CO_2 and 95% relative humidity. To assess cell targeting, Raji, Jurkat, Hut-78, or THP-1 cells (1×10^5) were incubated with fluorescence-labeled PEG (2×10^7), PEG-MS (2×10^7), or Doxil (0.44 μg based on lipid) nanoparticles with or without BsAb functionalization in complete RPMI-1640 media (100 μL) at 37 °C for 1 h. To assess CD20 and CD28 expression, CD20 AF647 (2H7, BioLegend) or CD28 AF647 (CD28.2, BioLegend) were incubated with cells at 4 °C for 1 h. After incubation, the cells were incubated on ice for 10 min, washed with flow cytometry staining (FACS) wash buffer (PBS containing 2 mM ethylenediaminetetraacetic acid and 0.5% w/v bovine serum albumin) twice, and analyzed by flow cytometry (LSRFortessa, BD Bioscience). The data were processed by using FlowJo V10. The degree of cell association of the particles was evaluated by using the percentage of cells that exhibited a stronger fluorescence intensity than control cells (untreated cells). Data were reported as the mean of three independent experiments with at least 40,000 cells analyzed for each experimental condition studied.

Whole Human Blood Model Spiked with B or T Cell Lines. Fresh human blood was collected from a healthy volunteer in sodium heparin vacuettes (Greiner Bio-One), and blood cells were counted with a CELL-DYN Emerald analyzer. Raji B cells and Jurkat T cells were labeled with a CellTrace yellow cell proliferation kit in PBS (1.5 μM) at 37 °C for 20 min and subsequently diluted and incubated with complete RPMI-1640 media for 5 min at 37 °C, followed by washing with complete RPMI-1640 media twice. Prelabeled Raji or Jurkat cells (1×10^5) were spiked into fresh human blood (100 μL), followed by the addition of fluorescence-labeled PEG (2×10^7), PEG-MS (2×10^7), or Doxil (0.44 μg based on lipid) nanoparticles with or without BsAb functionalization. After 1 h of incubation at 37 °C, whole blood was incubated on ice for 10 min, and red blood cells were lysed using Pharm Lyse buffer (4 mL) and removed by centrifugation (500*g*, 5 min). After being washed twice with FACS buffer, the cells were phenotyped at 4 °C for 1 h using an antibody cocktail consisting of antihuman CD3 AF700 (SP34−2, BD), CD14 APC-H7 (MΦP9, BD), CD66b BV421 (G10F5, BD), CD45 V500 (HI30, BD), CD56 PE-Cy7 (HCD56, BioLegend), lineage-1 (Lin-1) cocktail FITC (BD), HLA-DR PerCP-Cy5.5 (G46−6, BD), and CD19 BV650 (HIB19, BioLegend) in titrated concentrations. To assess CD20 and CD28 expression, CD20 AF647 or CD28 AF647 were incubated with cells at 4 °C for 1 h. The cells were subsequently washed twice with FACS wash buffer (4 mL, 500*g*, 7 min) to remove unbound antibodies and fixed with 4% paraformaldehyde in PBS and directly analyzed by flow cytometry. The data were processed using FlowJo V10. Cell association (%) refers to the proportion of each cell type with fluorescence above the background, stemming from fluorescence-labeled particles (see the gating strategy in Figure S3 and S4). Cell association (%) data are shown as the mean of three independent experiments (using fresh blood from each donor), with at least 400,000 leukocytes analyzed for each experimental condition studied.

CLL Patient Recruitment and Sample Collection. CLL patients were recruited through contacts with the investigators and invited to provide blood samples. For all participants, whole blood was collected with a sodium heparin anticoagulant. Plasma was collected and stored at −80 °C, and peripheral blood mononuclear

https://doi.org/10.1021/acsnano.4c09919
ACS Nano XXXX, XXX, XXX−XXX

cells (PBMCs) were isolated via Ficoll-Paque separation, cryopreserved in 10% dimethyl sulfoxide/FCS and stored in liquid nitrogen.

Whole Blood Model from CLL Patients. Fresh human blood was collected from CLL patients in sodium heparin vacuettes and counted with a CELL-DYN Emerald analyzer. The fresh blood (100 μL) was subsequently incubated with fluorescence-labeled PEG (2×10^7), PEG-MS (2×10^7), or Doxil (0.44 μg based on lipid) nanoparticles with or without BsAb functionalization at 37 °C for 1 h. After incubation, the whole blood was incubated on ice for 10 min, and red blood cells were lysed using Pharm Lyse buffer (4 mL) and removed by centrifugation (500*g*, 5 min). After being washed twice with FACS buffer, the cells were phenotyped at 4 °C for 1 h using an antibody cocktail consisting of antihuman CD3 AF700 (SP34−2, BD), CD14 APC-H7 (MΦP9, BD), CD66b BV421 (G10F5, BD), CD56 PE-Cy7 (HCD56, BioLegend), CD19 BV650 (HIB19, BioLegend), CD5 BV786 (UCHT2, BD), and CD22 PE (S-HCL-1, BD) in titrated concentrations. To assess CD20 and CD28 expression, antihuman CD20 AF647 (2H7, BioLegend) or CD28 AF647 (CD28.2, BioLegend) were incubated with cells at 4 °C for 1 h. The cells were subsequently washed twice with FACS wash buffer (4 mL, 500*g*, 7 min) to remove unbound antibodies and fixed with 4% paraformaldehyde in PBS and directly analyzed by flow cytometry. The data were processed using FlowJo V10. Cell association (%) refers to the proportion of each cell type with fluorescence above the background, stemming from fluorescence-labeled particles (see gating strategy in Figure S7). Cell association (%) data are shown as the mean ± SD of three independent experiments (using fresh blood from each donor), with at least 400,000 leukocytes analyzed for each experimental condition studied.

Confocal Microscopy Images of CLL PBMCs. Frozen PBMCs from a CLL patient were thawed, washed with RPMI 1640 (serum-free) media twice, and counted with a CELL-DYN Emerald analyzer. The washed PBMCs (3×10^6) were dispersed in RPMI 1640 (100 μL, serum-free) media, followed by the addition of human plasma (100 μL) from the same patient. AF555-labeled PEG-MS (2×10^7) or PEG (1.5×10^8) particles with or without BsAb functionalization were subsequently added into the PBMC suspension in the presence of human plasma and incubated at 37 °C for 1 h. Experiments at a lower PEG particle concentration (2×10^7) were also conducted. The dose of PEG particles was set at $1.5 \times 1 \times 10^8$ for optimal visualization of CLL targeting. After incubation, the cells were incubated on ice for 10 min, washed with FACS buffer (700*g*, 7 min), and phenotyped at 4 °C for 1 h using an antibody cocktail consisting of CD14 AF488 (M5E2, BD), CD20 AF647 (2H7, BioLegend), and CD3 BV421 (UCHT1, BioLegend) in titrated concentrations. The cells were subsequently washed with FACS wash buffer (4 mL, 700*g*, 7 min) and PBS (4 mL, 700*g*, 7 min), fixed with 4% paraformaldehyde in PBS (500 μL) for 20 min at 22 °C, then washed with PBS twice (3 mL, 1000*g*, 10 min), and finally mounted on an 8-well Lab-Tek chambered coverglass slide (Thermo Fisher Scientific, USA). The 8-well Lab-Tek chambered coverglass slide was pretreated with poly-L-lysine (200 μL, 0.01% w/v, M_w 70−150 kDa) solution for 14 h at 22 °C, followed by washing with PBS and air drying. The fixed cells were allowed to set in the dark for 12 h at 4 °C prior to imaging. Cells were imaged using a Nikon A1R+ confocal microscope with a 60×/1.4 NA Plan Apo λ oil immersion objective lens and 405, 488, 561, and 640 nm lasers.

Cytotoxicity of Nanoparticles in Whole Blood of CLL Patients. Fresh human blood was collected from CLL patients into sodium heparin vacuettes and counted with a CELL-DYN Emerald analyzer. The fresh blood (100 μL) was subsequently incubated with DiD-labeled Doxil nanoparticles (2.2 μg based on lipid, equivalent to 0.3 μg of doxorubicin) with or without BsAb functionalization at 37 °C for 24 h. Experiments at a lower Doxil dose (0.44 μg based on lipid, equivalent to 0.06 μg of doxorubicin) or a shorter incubation period (3 h) were also conducted to optimize the conditions. The dose of Doxil nanoparticles and the incubation period were set as 2.2 μg based on lipid (equivalent to 0.3 μg of doxorubicin) and 24 h for optimal cytotoxicity to CLL cells. After incubation, whole blood was incubated on ice for 10 min, and red blood cells were lysed using Pharm Lyse buffer (4 mL) and removed by centrifugation (500*g*, 5 min). After being washed twice with FACS buffer, the cells were phenotyped at 4 °C for 1 h using an antibody cocktail consisting of CD3 AF700 (SP34−2, BD), CD14 APC-H7 (MΦP9, BD), CD66b BV421 (G10F5, BD), CD56 PE-Cy7 (HCD56, BioLegend), CD19 BV650 (HIB19, BioLegend), CD5 BV786 (UCHT2, BD), and CD22 PE (S-HCL-1, BD) at titrated concentrations. To evaluate the cytotoxicity of Doxil, cells were incubated with a SYTOX AADvanced dead cell stain solution at a final concentration of 1 μM at 22 °C for 5 min, followed by storage on ice and direct analysis by flow cytometry. Dead cells were detected using an excitation wavelength of 488 nm, and emission was collected in a 695/40 bandpass. The data were processed using FlowJo V10. Live cell (%) refers to the proportion of each cell type without fluorescence above background, stemming from SYTOX AADvanced dead cell stain (see flow cytometry histogram examples in Figure 7a). Live cell (%) data are shown as the mean ± SD of three independent experiments (using fresh blood from each donor), with at least 400,000 leukocytes analyzed for each experimental condition studied.

Anti-PEG Antibody ELISA. An enzyme-linked immunosorbent assay (ELISA) was conducted to detect anti-PEG IgG and IgM using a previously developed method.[21] Briefly, the eight-arm PEG-NH_2 (40 kDa, 200 μg mL^{-1}, JenKem Technology, USA) in PBS was coated onto MaxiSorp 96-well plates (Nunc, Denmark) for 18 h at 4 °C, followed by washing with PBS four times. Plates were blocked with 5% (w/v) skim milk powder in PBS at 4 °C for 22 h, followed by adding serially diluted human plasma in 5% skim milk in duplicate for 1 h at 22 °C. Plates were washed with 0.1% 3-[(3-cholamidopropyl)-dimethylammonio]-1-propanesulfonate (Sigma-Aldrich, USA)/PBS buffer twice and PBS four times prior to addition of a Horseradish Peroxidase (HRP)-conjugated antihuman IgG (Dako Agilent, USA) at 1:20,000 dilution or HRP-conjugated antihuman IgM (Jackson ImmunoResearch Laboratories, USA) at 1:10,000 for 1 h at 22 °C. Plates were washed as above and then developed using 3,3′,5,5′-tetramethylbenzidine liquid substrate (Sigma-Aldrich, USA). Reaction was stopped with 0.16 M H_2SO_4, and the absorbance was measured at 450 nm. End point titers were calculated as the reciprocal plasma dilution giving signal 2× background using a fitted curve (4-parameter log regression) and reported as a mean of duplicates. Background was detected by adding the diluted plasma samples (at 1:10 dilution in 5% skim milk) to the non-PEG-coated wells, followed by the same ELISA procedure.

Statistical Analysis. The correlation analysis in Figure 6 and Figures S12−S15 was performed using nonparametric Spearman correlation tests in GraphPad Prism 10.2.2.

ASSOCIATED CONTENT

Supporting Information

The Supporting Information is available free of charge at https://pubs.acs.org/doi/10.1021/acsnano.4c09919.

Size and zeta potential of PEG, PEG-MS, and Doxil nanoparticles before and after functionalization with BsAbs; evaluation of cancer cell targeting using conventional cell line models; expression of CD20 and CD28 in blood immune cells from a healthy donor; gating strategy used to identify Raji/Jurkat cells and white blood cell population of the whole human blood model, wherein Raji/Jurkat cells are spiked into fresh whole blood of a healthy donor; cell count and expression of CD20 and CD28 in blood immune cells from CLL patients; gating strategy used to distinguish between CLL and normal B cells; gating strategy used to identify CLL cells and white blood cell population of the whole blood from CLL patients; Violin plots summarizing cell association (MFI) of BsAb-functionalized PEG, PEG-MS, and Doxil nanoparticles in the blood of CLL patients; Cell association (%) of BsAb-functionalized

https://doi.org/10.1021/acsnano.4c09919
ACS Nano XXXX, XXX, XXX−XXX

PEG-MS and Doxil particles in the whole blood of the 15 CLL patients; anti-PEG antibody levels in the plasma of CLL patients; correlation analysis between anti-PEG antibody levels and off-targeting association with blood phagocytes; correlation analysis between anti-PEG antibody levels and CLL targeting; correlation analysis between CD28/CD20 antigen expression on T/CLL cells and particle targeting performance (PDF)

AUTHOR INFORMATION

Corresponding Authors

Yi Ju − *School of Science, RMIT University, Melbourne, Victoria 3000, Australia; Department of Microbiology and Immunology, Peter Doherty Institute for Infection and Immunity, The University of Melbourne, Melbourne, Victoria 3000, Australia;* orcid.org/0000-0003-0103-1207; Email: david.ju@rmit.edu.au

Stephen J. Kent − *Department of Microbiology and Immunology, Peter Doherty Institute for Infection and Immunity, The University of Melbourne, Melbourne, Victoria 3000, Australia; Melbourne Sexual Health Centre and Department of Infectious Diseases, Alfred Hospital and Central Clinical School, Monash University, Melbourne, Victoria 3000, Australia;* orcid.org/0000-0002-8539-4891; Email: skent@unimelb.edu.au

Authors

Shiyao Li − *School of Science, RMIT University, Melbourne, Victoria 3000, Australia;* orcid.org/0000-0002-8053-7005

Abigail Er Qi Tan − *Department of Microbiology and Immunology, Peter Doherty Institute for Infection and Immunity, The University of Melbourne, Melbourne, Victoria 3000, Australia*

Emily H. Pilkington − *Department of Microbiology and Immunology, Peter Doherty Institute for Infection and Immunity, The University of Melbourne, Melbourne, Victoria 3000, Australia*

Paul T. Brannon − *Materials Characterisation and Fabrication Platform, The University of Melbourne, Parkville, Victoria 3010, Australia*

Magdalena Plebanski − *School of Health and Biomedical Sciences, RMIT University, Bundoora, Victoria 3083, Australia*

Jiwei Cui − *Key Laboratory of Colloid and Interface Chemistry of the Ministry of Education, School of Chemistry and Chemical Engineering, Shandong University, Jinan, Shandong 250100, China;* orcid.org/0000-0003-1018-4336

Frank Caruso − *Department of Chemical Engineering, The University of Melbourne, Parkville, Victoria 3010, Australia;* orcid.org/0000-0002-0197-497X

Kristofer J. Thurecht − *Australian Institute for Bioengineering and Nanotechnology, University of Queensland, St Lucia 4072, Australia;* orcid.org/0000-0002-4100-3131

Constantine Tam − *Department of Clinical Haematology, The Royal Melbourne Hospital and Peter MacCallum Cancer Centre, Melbourne, Victoria 3000, Australia; Faculty of Medicine, Dentistry and Health Sciences, The University of Melbourne, Melbourne, Victoria 3000, Australia*

Complete contact information is available at: https://pubs.acs.org/10.1021/acsnano.4c09919

Author Contributions

Y.J. and S.J.K. conceived, designed, and supervised the study and drafted the manuscript. Y.J., S.L., A.E.Q.T., E.H.P., and P.T.B. performed the experiments, analyzed the experiment data, and provided technical advice. Y.J., A.E.Q.T., C.T., and S.J.K. recruited the subjects and processed their blood samples. M.P., J.C., F.C., and K.J.T. provided intellectual input and reagents. All the authors approved the final version of the manuscript.

Notes

A version of this manuscript was posted to the preprint server *medRxiv* on May 31, 2024 as the following: Ju, Y.; Li, S.; Tan, A. E. Q.; Pilkington, E. H.; Brannon, P. T.; Plebanski, M.; Cui, J.; Caruso, F.; Thurecht, K. J.; Tam, C.; Kent, S. J. Ex Vivo Human Leukemia Blood Model Illustrates Limitations of Cancer-Targeting PEGylated Nanoparticles. *medRxiv* **2024**, DOI: 10.1101/2024.05.29.24308091 (accessed May 31, 2024). The authors declare no competing financial interest.

ACKNOWLEDGMENTS

We thank the participation of volunteers for their generous involvement and provision of blood samples. We thank D. Westerman, D. Ritchie, M. Dickinson, and A. Whitechurch (Peter MacCallum Cancer Centre) and R. Koldej (Royal Melbourne Hospital) for assistance with subject recruitment. We thank C.B. Howard and P. Huda (University of Queensland) for providing the BsAbs and T.H. Amarasena (University of Melbourne) for technical assistance. We acknowledge the Materials Characterisation and Fabrication Platform (MCFP) at The University of Melbourne for the use of the confocal microscopy and SIM. Transmission electron microscopy analyses were conducted using the facilities at the Biosciences Microscopy Unit, School of Bioscience, The University of Melbourne. We acknowledge the Ramaciotti Centre for Cryo-Electron Microscopy for instrument use. This study was supported by an Australian Research Council (ARC) Discovery Project (DP210103114 to F.C., S.J.K., Y.J.), an ARC Discovery Early Career Researcher Award (DE230101542, Y.J.), a Maxwell Eagle Endowment Award for Cancer Research (Y.J. and S.J.K.), an RMIT Vice-Chancellor's Postdoctoral Fellowship (Y.J.), an NHMRC program grant (GNT1149990, S.J.K. and F.C.), and NHMRC Investigator grants (S.J.K.; K.T.; and GNT2016732 to F.C.). Figures 2′a, 3a, and Table of Contents graphic were created with BioRender.com.

REFERENCES

(1) de Lázaro, I.; Mooney, D. J. Obstacles and Opportunities in a Forward Vision for Cancer Nanomedicine. *Nat. Mater.* **2021**, *20*, 1469−1479.

(2) Sharma, A.; Jasrotia, S.; Kumar, A. Effects of Chemotherapy on the Immune System: Implications for Cancer Treatment and Patient Outcomes. *Naunyn-Schmiedeberg's Arch. Pharmacol.* **2024**, *397*, 2551−2566.

(3) Fan, D.; Cao, Y.; Cao, M.; Wang, Y.; Cao, Y.; Gong, T. Nanomedicine in Cancer Therapy. *Signal Transduct. Target. Ther.* **2023**, *8*, 293.

(4) Moles, E.; Howard, C. B.; Huda, P.; Karsa, M.; McCalmont, H.; Kimpton, K.; Duly, A.; Chen, Y.; Huang, Y.; Tursky, M. L.; Ma, D.; Bustamante, S.; Pickford, R.; Connerty, P.; Omari, S.; Jolly, C. J.; Joshi, S.; Shen, S.; Pimanda, J. E.; Dolnikov, A.; et al. Delivery of PEGylated Liposomal Doxorubicin by Bispecific Antibodies Improves Treatment in Models of High-Risk Childhood Leukemia. *Sci. Transl. Med.* **2023**, *15*, No. eabm1262.

(5) Chen, H.-J.; Cheng, Y.-A.; Chen, Y.-T.; Li, C.-C.; Huang, B.-C.; Hong, S.-T.; Chen, I. J.; Ho, K.-W.; Chen, C.-Y.; Chen, F.-M.; Wang, J.-Y.; Roffler, S. R.; Cheng, T.-L.; Wu, T.-H. Targeting and Internalizing PEGylated Nanodrugs to Enhance the Therapeutic Efficacy of Hematologic Malignancies by Anti-PEG Bispecific Antibody (mPEG × CD20). *Cancer Nanotechnol.* **2023**, *14*, 78.
(6) Cui, J.; De Rose, R.; Alt, K.; Alcantara, S.; Paterson, B. M.; Liang, K.; Hu, M.; Richardson, J. J.; Yan, Y.; Jeffery, C. M.; Price, R. I.; Peter, K.; Hagemeyer, C. E.; Donnelly, P. S.; Kent, S. J.; Caruso, F. Engineering Poly(ethylene glycol) Particles for Improved Biodistribution. *ACS Nano* **2015**, *9*, 1571−1580.
(7) Dawson, K. A.; Yan, Y. Current Understanding of Biological Identity at the Nanoscale and Future Prospects. *Nat. Nanotechnol.* **2021**, *16*, 229−242.
(8) Ren, J.; Andrikopoulos, N.; Velonia, K.; Tang, H.; Cai, R.; Ding, F.; Ke, P. C.; Chen, C. Chemical and Biophysical Signatures of the Protein Corona in Nanomedicine. *J. Am. Chem. Soc.* **2022**, *144*, 9184−9205.
(9) Mahmoudi, M.; Landry, M. P.; Moore, A.; Coreas, R. The Protein Corona from Nanomedicine to Environmental Science. *Nat. Rev. Mater.* **2023**, *8*, 422−438.
(10) Corbo, C.; Molinaro, R.; Tabatabaei, M.; Farokhzad, O. C.; Mahmoudi, M. Personalized Protein Corona on Nanoparticles and Its Clinical Implications. *Biomater. Sci.* **2017**, *5*, 378−387.
(11) Yang, J.-L. J.; Narayanamurthy, R.; Yager, J. Y.; Unsworth, L. D. How Does Biological Sex Affect the Physiological Response to Nanomaterials? *Nano Today* **2021**, *41*, 101292.
(12) Nedelkov, D.; Kiernan, U. A.; Niederkofler, E. E.; Tubbs, K. A.; Nelson, R. W. Investigating Diversity in Human Plasma Proteins. *Proc. Natl. Acad. Sci. U.S.A.* **2005**, *102*, 10852−10857.
(13) Hadjidemetriou, M.; Mahmoudi, M.; Kostarelos, K. In Vivo Biomolecule Corona and the Transformation of a Foe into an Ally for Nanomedicine. *Nat. Rev. Mater.* **2024**, *9*, 219−222.
(14) Papi, M.; Caracciolo, G. Principal Component Analysis of Personalized Biomolecular Corona Data for Early Disease Detection. *Nano Today* **2018**, *21*, 14−17.
(15) Ren, J.; Cai, R.; Wang, J.; Daniyal, M.; Baimanov, D.; Liu, Y.; Yin, D.; Liu, Y.; Miao, Q.; Zhao, Y.; Chen, C. Precision Nanomedicine Development Based on Specific Opsonization of Human Cancer Patient-Personalized Protein Coronas. *Nano Lett.* **2019**, *19*, 4692−4701.
(16) Ju, Y.; Kelly, H. G.; Dagley, L. F.; Reynaldi, A.; Schlub, T. E.; Spall, S. K.; Bell, C. A.; Cui, J.; Mitchell, A. J.; Lin, Z.; Wheatley, A. K.; Thurecht, K. J.; Davenport, M. P.; Webb, A. I.; Caruso, F.; Kent, S. J. Person-Specific Biomolecular Coronas Modulate Nanoparticle Interactions with Immune Cells in Human Blood. *ACS Nano* **2020**, *14*, 15723−15737.
(17) Cui, J.; Ju, Y.; Houston, Z. H.; Glass, J. J.; Fletcher, N. L.; Alcantara, S.; Dai, Q.; Howard, C. B.; Mahler, S. M.; Wheatley, A. K.; De Rose, R.; Brannon, P. T.; Paterson, B. M.; Donnelly, P. S.; Thurecht, K. J.; Caruso, F.; Kent, S. J. Modulating Targeting of Poly(ethylene glycol) Particles to Tumor Cells Using Bispecific Antibodies. *Adv. Healthcare Mater.* **2019**, *8*, 1801607.
(18) Tung, H. Y.; Su, Y. C.; Chen, B. M.; Burnouf, P. A.; Huang, W. C.; Chuang, K. H.; Yan, Y. T.; Cheng, T. L.; Roffler, S. R. Selective Delivery of PEGylated Compounds to Tumor Cells by Anti-PEG Hybrid Antibodies. *Mol. Cancer Ther.* **2015**, *14*, 1317−1326.
(19) Sivaram, A. J.; Wardiana, A.; Alcantara, S.; Sonderegger, S. E.; Fletcher, N. L.; Houston, Z. H.; Howard, C. B.; Mahler, S. M.; Alexander, C.; Kent, S. J.; Bell, C. A.; Thurecht, K. J. Controlling the Biological Fate of Micellar Nanoparticles: Balancing Stealth and Targeting. *ACS Nano* **2020**, *14*, 13739−13753.
(20) Barenholz, Y. C. Doxil®—the First FDA-Approved Nano-Drug: Lessons Learned. *J. Controlled Release* **2012**, *160*, 117−134.
(21) Ju, Y.; Lee, W. S.; Pilkington, E. H.; Kelly, H. G.; Li, S.; Selva, K. J.; Wragg, K. M.; Subbarao, K.; Nguyen, T. H. O.; Rowntree, L. C.; Allen, L. F.; Bond, K.; Williamson, D. A.; Truong, N. P.; Plebanski, M.; Kedzierska, K.; Mahanty, S.; Chung, A. W.; Caruso, F.; Wheatley, A. K.; et al. Anti-PEG Antibodies Boosted in Humans by SARS-CoV-2 Lipid Nanoparticle mRNA Vaccine. *ACS Nano* **2022**, *16*, 11769−11780.
(22) Li, S.; Ma, Y.; Cui, J.; Caruso, F.; Ju, Y. Engineering Poly(ethylene glycol) Particles for Targeted Drug Delivery. *Chem. Commun.* **2024**, *60*, 2591−2604.
(23) Song, J.; Ju, Y.; Amarasena, T. H.; Lin, Z.; Mettu, S.; Zhou, J.; Rahim, M. A.; Ang, C.-S.; Cortez-Jugo, C.; Kent, S. J.; Caruso, F. Influence of Poly(ethylene glycol) Molecular Architecture on Particle Assembly and Ex Vivo Particle-Immune Cell Interactions in Human Blood. *ACS Nano* **2021**, *15*, 10025−10038.
(24) Tian, Y.; Gao, Z.; Wang, N.; Hu, M.; Ju, Y.; Li, Q.; Caruso, F.; Hao, J.; Cui, J. Engineering Poly(ethylene glycol) Nanoparticles for Accelerated Blood Clearance Inhibition and Targeted Drug Delivery. *J. Am. Chem. Soc.* **2022**, *144*, 18419−18428.
(25) Chen, B.-M.; Cheng, T.-L.; Roffler, S. R. Polyethylene Glycol Immunogenicity: Theoretical, Clinical, and Practical Aspects of Anti-Polyethylene Glycol Antibodies. *ACS Nano* **2021**, *15*, 14022−14048.
(26) Hadjidemetriou, M.; McAdam, S.; Garner, G.; Thackeray, C.; Knight, D.; Smith, D.; Al-Ahmady, Z.; Mazza, M.; Rogan, J.; Clamp, A.; Kostarelos, K. The Human in Vivo Biomolecule Corona onto PEGylated Liposomes: A Proof-of-Concept Clinical Study. *Adv. Mater.* **2019**, *31*, 1803335.
(27) Giulimondi, F.; Digiacomo, L.; Pozzi, D.; Palchetti, S.; Vulpis, E.; Capriotti, A. L.; Chiozzi, R. Z.; Laganà, A.; Amenitsch, H.; Masuelli, L.; Mahmoudi, M.; Screpanti, I.; Zingoni, A.; Caracciolo, G. Interplay of Protein Corona and Immune Cells Controls Blood Residency of Liposomes. *Nat. Commun.* **2019**, *10*, 3686.
(28) Dilliard, S. A.; Cheng, Q.; Siegwart, D. J. On the Mechanism of Tissue-Specific mRNA Delivery by Selective Organ Targeting Nanoparticles. *Proc. Natl. Acad. Sci. U.S.A.* **2021**, *118*, No. e2109256118.
(29) Qiu, M.; Tang, Y.; Chen, J.; Muriph, R.; Ye, Z.; Huang, C.; Evans, J.; Henske, E. P.; Xu, Q. Lung-Selective Mrna Delivery of Synthetic Lipid Nanoparticles for the Treatment of Pulmonary Lymphangioleiomyomatosis. *Proc. Natl. Acad. Sci. U.S.A.* **2022**, *119*, No. e2116271119.
(30) Salvati, A.; Pitek, A. S.; Monopoli, M. P.; Prapainop, K.; Bombelli, F. B.; Hristov, D. R.; Kelly, P. M.; Åberg, C.; Mahon, E.; Dawson, K. A. Transferrin-Functionalized Nanoparticles Lose Their Targeting Capabilities When a Biomolecule Corona Adsorbs on the Surface. *Nat. Nanotechnol.* **2013**, *8*, 137−143.
(31) Yao, X.; Qi, C.; Sun, C.; Huo, F.; Jiang, X. Poly(ethylene glycol) Alternatives in Biomedical Applications. *Nano Today* **2023**, *48*, 101738.
(32) Hoang Thi, T. T.; Pilkington, E. H.; Nguyen, D. H.; Lee, J. S.; Park, K. D.; Truong, N. P. The Importance of Poly(ethylene glycol) Alternatives for Overcoming PEG Immunogenicity in Drug Delivery and Bioconjugation. *Polymers* **2020**, *12*, 298.
(33) Ibrahim, M.; Shimizu, T.; Ando, H.; Ishima, Y.; Elgarhy, O. H.; Sarhan, H. A.; Hussein, A. K.; Ishida, T. Investigation of Anti-PEG Antibody Response to PEG-Containing Cosmetic Products in Mice. *J. Controlled Release* **2023**, *354*, 260−267.
(34) Gaballa, S. A.; Shimizu, T.; Takata, H.; Ando, H.; Ibrahim, M.; Emam, S. E.; Amorim Matsuo, N. C.; Kim, Y.; Naguib, Y. W.; Mady, F. M.; Khaled, K. A.; Ishida, T. Impact of Anti-PEG IgM Induced via the Topical Application of a Cosmetic Product Containing PEG Derivatives on the Antitumor Effects of PEGylated Liposomal Antitumor Drug Formulations in Mice. *Mol. Pharmaceutics* **2024**, *21*, 622−632.
(35) Ju, Y.; Carreño, J. M.; Simon, V.; Dawson, K.; Krammer, F.; Kent, S. J. Impact of Anti-PEG Antibodies Induced by SARS-CoV-2 mRNA Vaccines. *Nat. Rev. Immunol.* **2023**, *23*, 135−136.
(36) Armstrong, J. K.; Hempel, G.; Koling, S.; Chan, L. S.; Fisher, T.; Meiselman, H. J.; Garratty, G. Antibody against Poly(ethylene glycol) Adversely Affects PEG-Asparaginase Therapy in Acute Lymphoblastic Leukemia Patients. *Cancer* **2007**, *110*, 103−111.
(37) Hershfield, M. S.; Ganson, N. J.; Kelly, S. J.; Scarlett, E. L.; Jaggers, D. A.; Sundy, J. S. Induced and Pre-Existing Anti-Polyethylene Glycol Antibody in a Trial of Every 3-Week Dosing of

https://doi.org/10.1021/acsnano.4c09919
ACS Nano XXXX, XXX, XXX−XXX

Pegloticase for Refractory Gout, Including in Organ Transplant Recipients. *Arthrit. Res. Ther.* **2014**, *16*, R63.
(38) Lipsky, P. E.; Calabrese, L. H.; Kavanaugh, A.; Sundy, J. S.; Wright, D.; Wolfson, M.; Becker, M. A. Pegloticase Immunogenicity: The Relationship between Efficacy and Antibody Development in Patients Treated for Refractory Chronic Gout. *Arthrit. Res. Ther.* **2014**, *16*, R60.
(39) Liu, Y.; Smith, C. A.; Panetta, J. C.; Yang, W.; Thompson, L. E.; Counts, J. P.; Molinelli, A. R.; Pei, D.; Kornegay, N. M.; Crews, K. R.; Swanson, H.; Cheng, C.; Karol, S. E.; Evans, W. E.; Inaba, H.; Pui, C.-H.; Jeha, S.; Relling, M. V. Antibodies Predict Pegaspargase Allergic Reactions and Failure of Rechallenge. *J. Clin. Oncol.* **2019**, *37*, 2051−2061.
(40) Ju, Y.; Kim, C.-J.; Caruso, F. Functional Ligand-Enabled Particle Assembly for Bio-Nano Interactions. *Acc. Chem. Res.* **2023**, *56*, 1826−1837.
(41) Duggan, S. T.; Keating, G. M. Pegylated Liposomal Doxorubicin. *Drugs* **2011**, *71*, 2531−2558.
(42) Howard, C. B.; Fletcher, N.; Houston, Z. H.; Fuchs, A. V.; Boase, N. R. B.; Simpson, J. D.; Raftery, L. J.; Ruder, T.; Jones, M. L.; de Bakker, C. J.; Mahler, S. M.; Thurecht, K. J. Targeted Nanomaterials: Overcoming Instability of Antibody-Nanomaterial Conjugates: Next Generation Targeted Nanomedicines Using Bispecific Antibodies. *Adv. Healthcare Mater.* **2016**, *5*, 2055−2068.

https://doi.org/10.1021/acsnano.4c09919
ACS Nano XXXX, XXX, XXX−XXX